Photosynth Res
DOI 10.1007/s11120-017-0348-0

ORIGINAL ARTICLE

Characterization of Frex as an NADH sensor for in vivo applications in the presence of NAD^+ and at various pH values

Svea Wilkening[1] · Franz-Josef Schmitt[1] · Marius Horch[1] · Ingo Zebger[1] · Oliver Lenz[1] · Thomas Friedrich[1]

Received: 29 November 2016 / Accepted: 1 February 2017

Abstract The fluorescent biosensor Frex, recently introduced as a sensitive tool to quantify the NADH concentration in living cells, was characterized by time-integrated and time-resolved fluorescence spectroscopy regarding its applicability for in vivo measurements. Based on the purified sensor protein, it is shown that the NADH dependence of Frex fluorescence can be described by a Hill function with a concentration of half-maximal sensor response of $K_D \approx 4$ µM and a Hill coefficient of $n \approx 2$. Increasing concentrations of NADH have moderate effects on the fluorescence lifetime of Frex, which changes by a factor of two from about 500 ps in the absence of NADH to 1 ns under fluorescence-saturating NADH concentrations. Therefore, the observed sevenfold rise of the fluorescence intensity is primarily ascribed to amplitude changes. Notably, the dynamic range of Frex sensitivity towards NADH highly depends on the NAD^+ concentration, while the apparent K_D for NADH is only slightly affected. We found that NAD^+ has a strong inhibitory effect on the fluorescence response of Frex during NADH sensing, with an apparent NAD^+ dissociation constant of $K_I \approx 400$ µM. This finding was supported by fluorescence lifetime measurements, which showed that the addition of NAD^+ hardly affects the fluorescence lifetime, but rather reduces the number of Frex molecules that are able to bind NADH. Furthermore, the fluorescence responses of Frex to NADH and NAD^+ depend critically on pH and temperature. Thus, for in vivo applications of Frex, temperature and pH need to be strictly controlled or considered during data acquisition and analysis. If all these constraints are properly met, Frex fluorescence intensity measurements can be employed to estimate the minimum NADH concentration present within the cell at sufficiently low NAD^+ concentrations below 100 µM.

Keywords Fluorescence sensor protein · Redox sensing · NADH · NAD^+ · Frex · Decay-associated spectra · Fluorescence lifetime · Light-driven biohydrogen production

Abbreviations

ADP	Adenosine diphosphate
cpFP	Circularly permuted fluorescent protein
cpYFP	Circularly permuted yellow fluorescent protein
DAS	Decay-associated spectra
eGFP	Enhanced green fluorescent protein
DNA	Desoxyribonucleic acid
Frex	Fluorescent Rex
FrexH	Frex of high affinity
IPTG	Isopropyl β-D-1-thiogalactopyranoside
LB	Luria Bertani
NAD	Nicotinamide adenine dinucleotide
NAD^+	Oxidized nicotinamide adenine dinucleotide
N^+	NAD^+
NADH	Reduced nicotinamide adenine dinucleotide
N	NADH
NADP	Nicotinamide adenine dinucleotide phosphate
NADPH	Reduced nicotinamide adenine dinucleotide phosphate
$NADP^+$	Oxidized nicotinamide adenine dinucleotide phosphate
OD	Optical density

Electronic supplementary material The online version of this article (doi:10.1007/s11120-017-0348-0) contains supplementary material, which is available to authorized users.

✉ Franz-Josef Schmitt
schmitt@physik.tu-berlin.de

[1] Institut für Chemie, Technische Universität Berlin, Sekr. PC 14, Straße des 17. Juni 135, Berlin 10623, Germany

Published online: 06 March 2017

PBS	Phosphate-buffered saline
ROS	Reactive oxygen species
rpm	revolutions per minute
TWCSPC	Time- and wavelength-correlated single photon counting
YFP	Yellow fluorescent protein

Introduction

The reduced and oxidized forms of nicotinamide adenine dinucleotide (NADH and NAD^+) as well as their phosphorylated congeners (NADPH and $NADP^+$) are involved in many important metabolic reactions in all living organisms (for a recent review, see Ying 2008). While NAD plays a major role in catabolic reactions (Lin and Guarente 2003), NADP represents a central cofactor of the cellular anabolism, and both NAD and NADP are involved in the generation and detoxification of reactive oxygen species. Consequently, they play an important role in photosynthetic organisms, as outlined in a recent review (Schmitt et al. 2014a). Moreover, in biotechnological approaches to light-driven hydrogen production, [NADPH]/[$NADP^+$] and [NADH]/[NAD^+] ratios may serve as key determinants and indicators for hydrogen production by hydrogenases (Yacoby et al. 2011; Lenz et al. 2015). Therefore, it is of interest to probe these metabolites in vivo as well as in vitro, and in the current account, we will focus on the monitoring of the non-phosphorylated forms.

A rather straightforward approach to quantify NADH is based on the direct measurement of its weak autofluorescence (Rocheleau et al. 2004). Unfortunately, this method neither allows for the discrimination between NADH and its phosphorylated congener, NADPH, nor does it distinguish between protein-bound and free nucleotides (Blacker et al. 2014). In addition, the oxidized nucleotide (NAD^+), which is non-fluorescent, cannot be evaluated by this method, and a significant background of cellular autofluorescence during measurements complicates its application in vivo (Patterson et al. 2000).

Various alternative approaches to determine cellular NADH and NAD^+ levels were conceptualized, such as enzyme cycling assays, mass spectrometry, and high performance liquid chromatography (Bilan and Belousov 2016). All of these methods, however, require cell disruption; therefore, both the in vivo quantification of these metabolites and, as mentioned above, the discrimination between protein-bound and free nucleotides are impossible.

An alternative method to dynamically monitor the NAD(H) level in living cells focuses on genetically encoded fluorescent sensors that respond to [NADH] or the [NADH]/[NAD^+] ratio (Hung et al. 2011; Zhao et al. 2011, 2015; Bilan et al. 2014). Several fluorescent NAD(H) sensors have been developed by fusing parts of a bacterial [NADH]/[NAD^+] sensing repressor from the Rex protein family into the sequence of circularly permuted fluorescent proteins (cpFPs). CpFPs exhibit new C- and N-termini that are in close proximity to the chromophore, which in turn makes these fluorescent proteins more sensitive towards structural changes (Baird et al. 1999). The Rex protein itself is a homodimer, which consists of a DNA-binding N-terminal domain and a nucleotide-binding C-terminal domain containing a Rossman fold (Brekasis and Paget 2003; Sickmier et al. 2005). If the [NADH]/[NAD^+] ratio is low, the protein binds to DNA and represses the expression of certain enzymes, with one molecule NAD^+ bound (Larsson et al. 2005; Gyan et al. 2006; McLaughlin et al. 2010). At increased [NADH]/[NAD^+] ratios, Rex binds two NADH molecules (one in each C-terminal domain of the dimer), which in turn induces a dramatic structural change and a subsequent dissociation of Rex from the DNA, eventually permitting the expression of the target proteins (Sickmier et al. 2005). For the generation of fluorescent probes, the structural transformations of Rex in response to NADH binding have been exploited in order to generate biosensors that change their fluorescence in response to the NAD(H) level (Hung et al. 2011; Zhao et al. 2011, 2015; Bilan et al. 2014).

Following this approach, several biosensors have been developed, one of the first of which was the Peredox sensor. In Peredox, a T-Rex (Rex protein from *Thermus aquaticus*) tandem dimer was fused to a circularly permuted T-Sapphire fluorescent probe (Hung et al. 2011). The resulting sensor was able to accurately report changes in the [NADH]/[NAD^+] ratio in several eukaryotic cell lines. In contrast, Peredox was proven to be unsuitable for monitoring the [NADH]/[NAD^+] ratio in mitochondria (Hung et al. 2011) as well as bacteria (Tejwani et al. 2016). In these cases, the NADH concentrations clearly exceeded the sensitivity range of the sensor, so that its fluorescence response was saturated and unable to report metabolic changes.

In another study, Zhao et al. presented sensors of similar design, based on a B-Rex (Rex protein from *Bacillus subtilis*) fused to a circularly permuted yellow fluorescent protein (cpYFP). These sensors, termed Frex (fluorescent Rex) and FrexH (Frex of high affinity), were reported to respond to NADH (Zhao et al. 2011) but not to NAD^+ and other structurally related nucleotides. Moreover, they were described as inherently ratiometric, therefore providing the possibility to detect NADH levels independent from the expression level in a particular cell. Using 480 nm excitation, Frex fluorescence properly reported the NADH concentration in vitro, and its rapid response to and high specificity for NADH were suggested to be promising for further utilization in vivo. However, the fluorescence response of Frex has not been explored systematically in

the simultaneous presence of NADH and NAD^+, a situation to be expected in vivo.

In this work, we carried out a characterization of Frex by fluorescence spectroscopy of the purified sensor protein in order to characterize its response in the simultaneous presence of NAD^+ and NADH. The effect of pH variations and temperature on the sensor's fluorescence was also elucidated, and all results were analysed with respect to Frex's potential applicability for in vivo measurements.

Materials and methods

All chemicals used in this study were at least at analytical grade. NAD^+ and NADH disodium salts were purchased from Applichem (Darmstadt, Germany).

Expression and purification of Frex

Escherichia coli BL21 (DE3) pLysS cells were transformed with the $pRSET_B$ plasmid harbouring the Frex cDNA in tandem with an N-terminal His-tag (Zhao et al. 2011). Cells were grown in 1 L of LB medium containing 100 µg/mL ampicillin and 34 µg/mL chloramphenicol at 37 °C and 220 rpm until the culture reached an OD_{600} of 0.6. Expression of the protein was induced by addition of 0.5 mM IPTG, and cells were subsequently grown at 18 °C for 48 h. The cells were harvested at 5000×*g* for 10 min at 4 °C and resuspended in lysis buffer [PBS (137 mM NaCl, 2.7 mM KCl, 10 mM Na_2HPO_4, 1.8 mM KH_2PO_4, pH 7.4) containing Complete® protease inhibitor (Roche Molecular Biochemicals, Mannheim, Germany) and 100 mg/mL lysozyme]. The cells were lysed by three subsequent freeze/thaw cycles. The lysed cells were centrifuged (18.000×*g*, 10 min, 4 °C), and the supernatant was filtered. The cleared lysate was loaded onto a cobalt affinity column (HiTrap™ TALON® crude 5 mL, GE Healthcare Europe GmbH, Freiburg, Germany), which was previously equilibrated. The sample was washed three times and eluted with 300 mM imidazole. The eluted fraction was concentrated to 2.5 mL, and imidazole was removed by loading the sample onto a desalting column (PD-10 desalting column, GE Healthcare, Little Chalfont, UK). The purified protein was collected, and aliquots were snap-frozen in liquid nitrogen and stored at −80 °C until further usage. The protein concentration was evaluated by a Bradford assay.

Fluorescence intensity measurements

NADH titration studies were performed with a commercial USB-connected fluorometer system with a CCD array (EPP2000, Scientific Instruments, Berlin, Germany) providing a spectral resolution of 3 nm. Excitation was performed with a pulsed 470 nm laser diode (LDH-470, Picoquant, Berlin, Germany). The spectrometer was set to monitor the whole spectral range between 400 and 800 nm. The emission below 490 nm was blocked by a 488-nm longpass filter (F-76-490, AHF Analysentechnik, Tübingen, Germany). For nucleotide titration studies, a 500 nM protein solution was prepared in PBS (pH 7.4), and nucleotides were added to the denoted concentrations.

The titration data were evaluated by fits of a Hill function:

$$F = \frac{F_{\max}[\mathrm{NADH}]^n}{K_D^n + [\mathrm{NADH}]^n}. \quad (1)$$

Here, $F_{\max}$ is the fluorescence obtained at saturating NADH concentrations, K_D is the (apparent) average microscopic dissociation constant (the NADH concentration necessary for half-maximal sensor response), and n is the Hill coefficient. For these calculations and data presentation Origin 8.0 was used (OriginLab Corp., Northampton, MA, U.S.A.). The activation of Frex by NADH (Fig. 1), the time-resolved emission (Fig. 3), and the inhibition of Frex by NAD^+ (Fig. 4) were measured at 20 °C. Data are presented as means ± standard deviation.

For the analysis of the pH dependence and NAD^+ titration studies, the fluorescence was measured with a Fluoromax-2 spectro-fluorometer (Horiba Jobin Yvon, Bensheim, Germany). Frex was excited at 480 nm using a Xenon lamp with a monochromator, and emission spectra were recorded from 490 to 600 nm at 30 °C (Figs. 2, 5). The UV/vis absorption spectrum of Frex is shown in Supplementary material Fig. S1. Slits were set to 4 nm for excitation and 2 nm for emission, while the integration time was 1 s and the increment 1 nm. For nucleotide titration studies, a 500 nM Frex solution was prepared in PBS (pH 7.4), and nucleotides were added to the denoted concentrations. For measurements of the pH effect on Frex fluorescence, also 500 nM of protein was resuspended in different PBS buffer solutions adjusted to the desired pH.

Time- and wavelength-correlated single photon counting (TWCSPC)

TWCSPC measurements were performed employing a Hamamatsu R5900 16-channel multi-anode photomultiplier tube (PMT) with 16 separate output (anode) elements and a common cathode and dynode system (PML-16C, Becker&Hickl, Berlin, Germany). The polychromator was equipped with a 300 grooves/mm grating resulting in a spectral bandwidth of the PML-16C of 12.5 nm/channel. A 470 nm pulsed laser diode (LDH-470, Picoquant, Berlin, Germany) delivering 60 ps FWHM pulses, driven at a repetition rate of 20 MHz, was used for excitation. The fluorescence was observed via

a 488 nm longpass filter (F-76-490, AHF Analysentechnik, Tübingen, Germany).

Determination of decay-associated spectra (DAS)

The fluorescence decay was analysed employing a Levenberg–Marquardt algorithm for the minimization of the reduced $\chi_r^2(\lambda)$ in each wavelength section. The influence of the instrumental response function (IRF), which is the registered response to scattered laser pulses, is considered during the fitting procedure as the determined biexponential decay is convoluted with the IRF before comparison with the measured data and the calculation of $\chi_r^2(\lambda)$. The value of $\chi_r^2(\lambda)$ depends on a parameter set $(p_1, \ldots, p_n)$ of the chosen continuous mathematical function $A(t, \lambda, p_1, \ldots, p_n)$ for the measured fluorescence intensity $F(t_\nu, \lambda)$ in each time channel t_ν.

The function $\chi_r^2(\lambda)$ is evaluated for each time t_ν channel ($\nu = 1 \ldots 4096$) after convolution of the function $A(t, \lambda, p_1, \ldots, p_n)$ with the IRF, which delivers the fit function

$$F^{\text{fit}}(t_\nu, \lambda) = \int A(t, \lambda, p_1, \ldots, p_n) \cdot \text{IRF}(t_\nu - t)\,\mathrm{d}t \tag{2}$$

and averaged over all time channels:

$$\chi_r^2(\lambda) = \sum_{\nu=1}^{4096} \frac{1}{(N-n-1)} \left(\frac{F(t_\nu, \lambda) - F^{\text{fit}}(t_\nu, \lambda)}{\sqrt{F(t_\nu, \lambda)}} \right)^2. \tag{3}$$

Equation 2 is based on the assumption that the number of photons registered in each time channel t_ν follows a Poisson distribution so that the standard deviation σ in each channel equals the square root of the fluorescence intensity $\sigma(t_\nu, \lambda) = \sqrt{F(t_\nu, \lambda)}$. N determines the full number of data points (here 4096 for each wavelength section λ) and n the size of the parameter set for the chosen mathematical function $A(t, \lambda, p_1, \ldots, p_n)$, which was assumed to be a biexponential decay function

$$A(t, \lambda) = \sum_{j=1}^{2} a_j(\lambda)\ \mathrm{e}^{-t/\tau_j} \tag{4}$$

with the parameters $a_j(\lambda)$ and τ_j denoting the wavelength-dependent amplitude and the time constant of the jth exponential decay component for two components ($n = 2$), respectively. The biexponential fits of all decay curves measured in one time- and wavelength-resolved fluorescence spectrum were performed as global fits with common values of lifetimes τ_j for all decay curves (linked parameters) and wavelength-dependent pre-exponential factors $a_j(\lambda)$ (non-linked parameters). The result of this analysis is usually plotted as a graph of $a_j(\lambda)$ for all wavelength-independent lifetimes τ_j under the constraint that $a_1 + a_2 = 1$ in the fluorescence maximum, representing so called normalized decay-associated spectra (DAS) that reveal the spectral distribution of individual decay components. For this calculation, the software of Globals Unlimited® (University of Illinois, Urbana, USA) was used.

Results

NADH titration experiments

Frex was purified after expression in *E. coli*, and its in vitro response towards NADH as well as NAD^+ was measured with fluorescence spectroscopy. Since the fluorescence emission upon excitation at 400 nm changed only slightly when adding NADH, no further ratiometric measurements were performed, and only the fluorescence signals obtained during excitation at 470 nm were used for analysis. The purified protein was titrated with NADH in the range of 0–200 µM, first, in the absence of NAD^+ and, second, in the presence of 1 mM NAD^+ (see Fig. 1).

In the absence of NAD^+, Frex is supposed to exhibit a maximal dynamic range in response to NADH (Fig. 1 left), since it has been reported to be a selective sensor for NADH (Zhao et al. 2011, 2016). Consistently, the sensor showed a sevenfold larger fluorescence amplitude (600% dynamic range) compared to the value observed without NADH, and the maximum (saturation of the sensor's response) was reached above 50 µM NADH. In vivo, however, NADH and NAD^+ are simultaneously present, and the [NADH]/[NAD^+] ratio, rather than the absolute NADH concentration, reflects the metabolic state of the cell. Thus, we also characterized the dependency of Frex on [NADH] and [NAD^+] by measuring the response to NADH in the presence of 1 mM NAD^+ (Fig. 1 right), a typical concentration found in bacteria (Bennett et al. 2009; Zhou et al. 2011; Tejwani et al. 2016). Under these conditions, the maximum fluorescence increase is only fourfold (300% dynamic range), i.e. it is diminished to about 60% of the value obtained without NAD^+ (compare Fig. 1 left and right). By contrast, in the presence of 100 µM NAD^+, a concentration typically expected for mammalian cells, the response of Frex to NADH is comparable to that observed in the absence of NAD^+ (see Supplementary material Fig. S2). The data of Fig. 1 and Supplementary material Fig. S2 can be well fit by Hill functions, thereby providing (apparent) average microscopic dissociation constants, K_D, as well as insights into the possible cooperativity of the NADH binding process. In the absence of NAD^+, K_D was determined to be 3.5 ± 0.3 µM, while in the presence of 100 µM and 1 mM NAD^+, the apparent K_D was 4.4 ± 0.3 and 9.7 ± 0.7 µM, respectively. The corresponding Hill coefficients n were 1.9 ± 0.2, 1.5 ± 0.2, and 1.6 ± 0.2, respectively. Assuming that one Frex molecule (containing

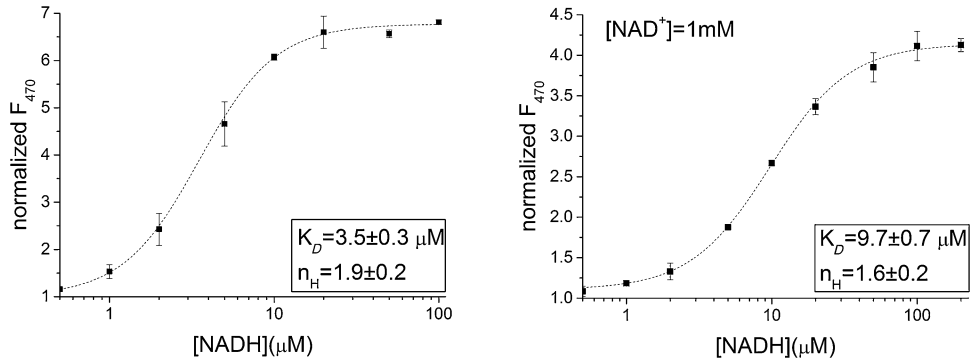

Fig. 1 Fluorescence responses of the purified Frex sensor protein, expressed as the fluorescence amplitudes at 515 nm measured upon 470 nm (F_{470}) excitation at different [NADH] in the absence of NAD^+ (*left*) or the presence of 1 mM NAD^+ (*right*). The fluorescence signals were normalized to F_{470} measured in the absence of NADH. The concentration of the sensor protein was 500 nM. The superimposed dashed lines represent fits of a Hill function to the data, with the resulting fit parameters shown in the *insets*. Experiments were performed at 20 °C

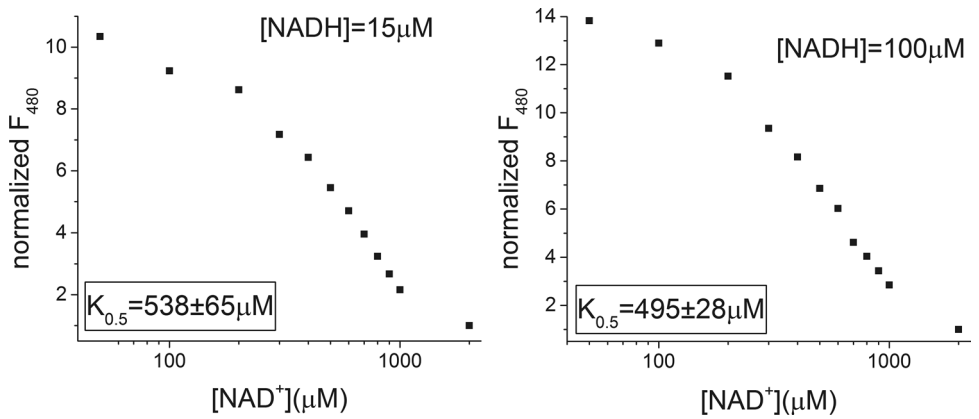

Fig. 2 Fluorescence responses of the purified Frex sensor protein, expressed as the fluorescence amplitudes measured upon 480 nm excitation (F_{480}) at different [NAD^+] in the presence of 15 μM NADH (*left*) or 100 μM NADH (*right*). The fluorescence intensity was normalized to F_{480} in the presence of 2 mM NAD^+. The concentration of the sensor protein was 500 nM. Experiments were carried out at 30 °C, and thus data cannot be quantitatively compared to those of Fig. 1

a tandem dimer of a Rex repressor protein) can bind two molecules of NADH (vide supra), this indicates nearly perfect cooperativity, as may be expected for a multimeric protein like Frex (Zhao et al. 2011).

Since our data suggest a dramatic dependence of Frex fluorescence and dynamic range on the NAD^+ concentration, the response of Frex to varying NAD^+ concentrations in the presence of fixed amounts of NADH (15 and 100 μM) was investigated as well (Fig. 2). For the representation of these data, the fluorescence responses measured upon 480 nm excitation were calculated. In accordance with the above observations, these experiments demonstrate that Frex fluorescence amplitudes decrease significantly with increasing NAD^+ concentrations. The concentration of NAD^+ at which the fluorescence amplitude at a given NADH concentration decreased to half of its starting value ([NAD^+] = 0) was determined to be ca. 500 μM (Fig. 2).

Time-resolved fluorescence measurements

The reduction of the fluorescence amplitude with increasing NAD^+ concentration (see Fig. 2) raised questions about the exact mechanism of the Frex fluorescence response in the presence of both NADH and NAD^+. Notably, possible static and dynamic interactions between Frex and NAD^+ can be discriminated by time-resolved fluorescence spectroscopy, and this technique could also reveal how NAD^+ acts as an inhibitor for NADH sensing. To elucidate these issues, we first recorded the fluorescence decays at different wavelengths in order to calculate DAS for the fluorescence of Frex at varying concentrations of NADH upon excitation

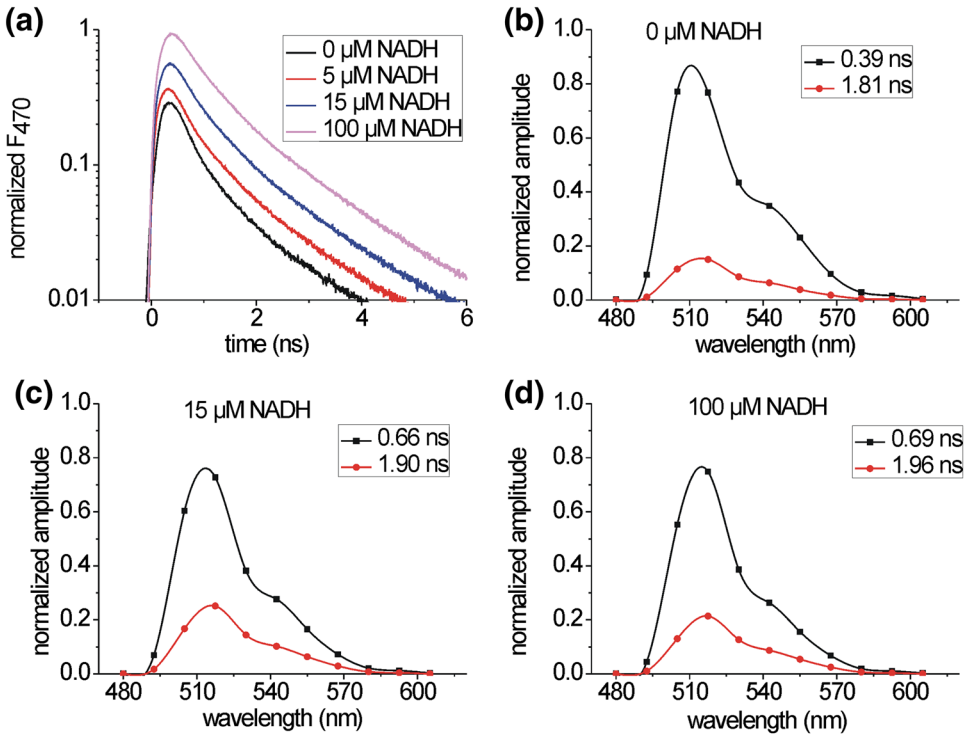

Fig. 3 **a** Fluorescence decays at 520 nm, near the emission maximum of Frex, obtained in the absence (*black curve*) and presence of NADH (*coloured curves*) upon excitation with a pulsed 470 nm laser source. To normalize the spectra, the maximum of the decay curve obtained at 100 µM NADH was set to unity, and all other curves were scaled accordingly. **b–d** DAS from global fits of a two-exponential model function (*red* and *black* data points), which yielded two global decay time constants (values are given in the *insets*) and the corresponding amplitudes a_1 and a_2 (normalized to $a_1 + a_2 = 1$) for the fluorescence decay curves of Frex measured in the absence (**b**) and presence of 15 µM (**c**) or 100 µM (**d**) NADH. Experiments were performed at 20 °C

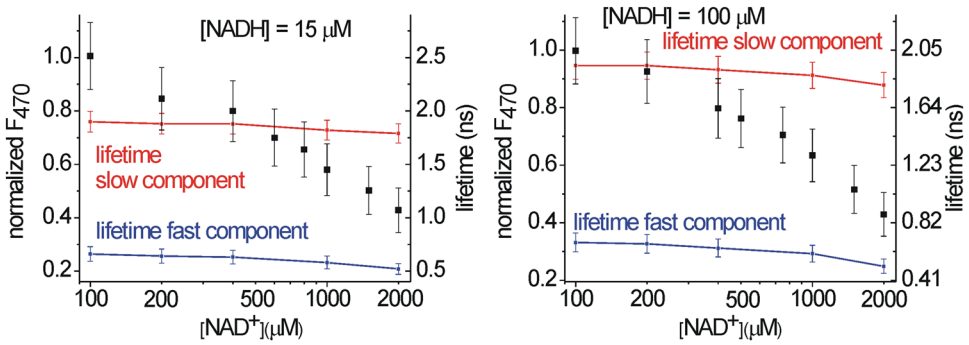

Fig. 4 Titration of Frex with different concentrations of NAD^+ in the presence of 15 (*left*) or 100 µM NADH (*right*). Changes of the lifetimes of the two decay components (*red* and *blue*) are compared to the simultaneously monitored overall fluorescence (*black squares*). Fluorescence was measured at 20 °C

with a pulsed 470 nm laser source using time- and wavelength-resolved single photon counting instrumentation.

Figure 3a shows that the initial amplitude (intensity at $t=0$) of the Frex emission rises upon addition of NADH, and at saturating NADH levels ([NADH] = 100 µM), an about fourfold increase is observed. Figure 3b–d displays the DAS for the whole spectral range between 480 and 605 nm obtained by global fitting of two exponential decay components to the time- and wavelength-resolved data recorded in the absence (Fig. 3b) and presence of NADH (Fig. 3c, d). The distribution of the different lifetime components is visualized by normalizing the amplitudes a_1 and a_2 of both spectral components to $a_1 + a_2 = 1$ near the fluorescence maximum at 515 nm. In the absence of NADH (Fig. 3b), the two-component fit reveals a first species with a lifetime of $\tau_1 = 1.8$ ns and a fractional amplitude of $a_1 = 0.12$ and a second species with $\tau_2 = 380$ ps and $a_2 = 0.88$. The resulting average lifetime $\bar{\tau} = a_1\tau_1 + a_2\tau_2$ is 550 ps. After adding NADH to a final concentration of 100 µM, the DAS are composed of a first component with a lifetime of $\tau_1 = 2.0$ ns and a fractional amplitude of $a_1 = 0.2$ and a second component with $\tau_2 = 0.7$ ns and $a_2 = 0.8$. Therefore, the average lifetime, resulting from these values, increases to about 1 ns, which is nearly twice the value obtained without NADH. Together with the increased initial amplitude, this leads to a total fluorescence gain by a factor of 7–8. Interestingly, the fluorescence lifetime depends on the NADH concentration in a biphasic fashion. The lifetime changes are completed at 15 µM NADH, and addition of more NADH yields no further changes (see Fig. 3c, d). In contrast, the fluorescence amplitude levels out at higher NADH concentrations of about 100 µM NADH (Fig. 3a, see also Fig. 1). According to these results, the increase of Frex fluorescence by NADH binding

appears to mainly result from "fluorescence activation" of the sensor molecules, i.e. an increased initial fluorescence amplitude after addition of NADH. Therefore, it is assumed that Frex molecules, which do not have bound NADH, are not contributing to the fluorescence signal, while Frex that bound two NADH molecules represents the dominant fluorescent species (for a scheme of Frex and the interaction with its cofactor NADH see Supplementary material Fig. S3).

Upon addition of increasing concentrations of NAD^+ (0–2 mM), the aforementioned fluorescence lifetimes did not vary significantly. To visualize this effect, Fig. 4 displays the lifetime changes of the fast (*blue*) and slow (*red*) decay components of Frex fluorescence in the presence of 15 µM (*left*) and 100 µM (*right*) NADH. In addition, the overall fluorescence intensity changes are also depicted (*black*), revealing a strong intensity decrease upon addition of NAD^+.

pH and temperature dependence of Frex fluorescence

Frex is based on the circularly permuted YFP, whose fluorescence emission exhibits a pronounced pH dependence (Schwarzländer et al. 2014). Therefore, as already noted by Zhao et al., Frex is also pH dependent (Zhao et al. 2011). In order to investigate the effect of pH, the fluorescence of the purified Frex sensor was measured in buffer solutions equilibrated to pH values between 7 and 10.5 in the absence of NADH. In Fig. 5, the corresponding fluorescence amplitudes of Frex after excitation at 480 nm are depicted. Notably, the fluorescence response at pH 10.5 is about 47-times higher than at pH 7, indicating that the dynamic range of the sensor is not yet fully utilized at pH 7.4 (only sevenfold increase upon NADH addition). Even more, this shows that extreme care has to be taken to avoid minute pH changes in the cell system under study. At physiological pH (which is around neutral in most cell types) even pH changes by few 0.1 units may obscure NAD(H)-dependent variations of the fluorescence response. Specifically, the fluorescence amplitude changes by a factor of 4.5 between pH 7 and 8.5 (Fig. 5, *inset*).

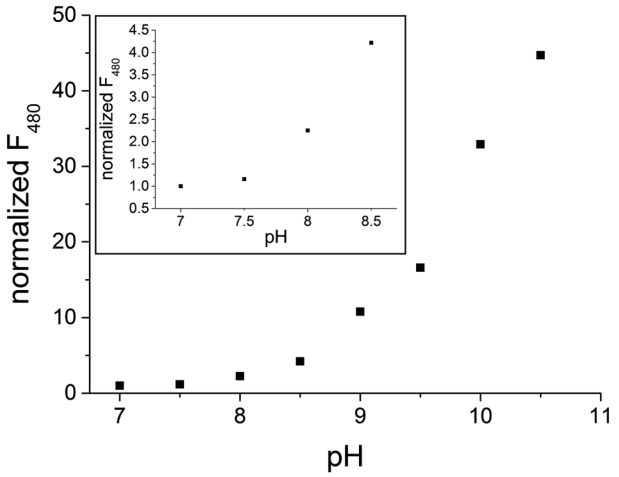

Fig. 5 Fluorescence responses of the purified Frex sensor protein, expressed as the fluorescence amplitudes measured upon 480 nm excitation (F_{480}), at different pH values in the absence of NADH and NAD^+. The fluorescence amplitudes were normalized to the maximum of F_{480} at pH 7. The *inset* shows normalized fluorescence amplitudes for the range between pH 7 and 8.5. The concentration of the sensor protein was 500 nM. Experiments were carried out at 30 °C

It should also be noted that Frex displays a pronounced temperature sensitivity, as expected for a sensor whose response is governed by analyte binding equilibria. We recognized a fourfold change in fluorescence amplitudes when comparing titrations of NAD^+ performed at 30 °C (as shown in Figs. 2, 5) and 20 °C (data of Figs. 1, 3, 4) at the same NADH concentration. This, of course, needs to be considered when comparing data obtained at different temperatures, e.g. in vivo and in vitro. Since the temperature range in which Frex is to be utilized depends on the cell line under study, a detailed characterization of the temperature dependence of the NAD^+/NADH binding equilibria is necessary.

Discussion

The physiological importance of intracellular concentrations of key metabolites, such as nicotinamide adenine dinucleotide, has inspired many different approaches to quantify these molecules in living systems. In this respect, recently developed genetically engineered fluorescence sensors are promising tools to explore NADH and/or NAD^+ concentrations in vivo.

The fluorescence sensor Frex was initially described to report [NADH] rather than the physiologically more important [NADH]/[NAD^+] ratio (Zhao et al. 2011). Nevertheless, in a recent study, the same authors reported slightly different Frex fluorescence responses in the presence or absence of 100 µM NAD^+, the latter of which was supposed to reflect the NAD^+ concentration in mammalian cells (Zhao et al. 2016). The authors concluded that this effect can be neglected for applications in such cells, since the sensor's response was not drastically altered (Zhao et al. 2016).

While this is in line with our observations (Supplementary material Fig. S2), we found that Frex exhibits a dramatically decreased dynamic range at higher NAD^+ concentrations (Fig. 1), which can falsify the readout of the probe. Therefore, for applications of Frex in bacterial cells, the NAD^+ concentration and its effect on Frex fluorescence need to be considered, since concentrations of this

metabolite are generally higher than in mammalian cells (Bennett et al. 2009; Tejwani et al. 2016).

To further investigate the interaction between NAD^+ and Frex, we recorded time-resolved fluorescence data, which showed that the fluorescence lifetime is hardly affected by the NAD^+ concentration. This excludes any form of dynamic quenching as an explanation for the observed properties, and fluorescence lifetime measurements cannot be used to discriminate between the sensor's response in the absence or presence of NAD^+. However, while the presence of NADH increased the fluorescence amplitude, NAD^+ apparently acted like a static quencher and decreased the fluorescence amplitudes. The time-integrated fluorescence amplitudes showed that, for a given NADH concentration, the maximal fluorescence response could only be detected in the absence of NAD^+. Notably, the parental protein Rex is a sensor for the [NADH]/[NAD^+] poise; therefore, it is not surprising that Rex has been described to bind both NADH and NAD^+ (Sickmier et al. 2005). Rex is generally believed to interact with two NADH molecules per dimer, but only one NAD^+ molecule (Sickmier et al. 2005). Binding of a single NAD^+ molecule to Rex, which occurs at a slightly different site, does not induce the conformational changes observed upon NADH binding (McLaughlin et al. 2010). Applied to Frex, the binding of NAD^+ would therefore not lead to a rise in fluorescence, since the conformational change underlying fluorescence activation does not occur (McLaughlin et al. 2010; Zhao et al. 2011). Thus, NAD^+ binding to Frex diminishes the concentration of the free sensor, which is able to readily bind two NADH molecules, and thus decreases the fluorescence response at a given NADH concentration.

These findings (Sickmier et al. 2005; Wang et al. 2008; McLaughlin et al. 2010) prompted us to describe NAD^+ (N^+) and NADH (N) interaction with Frex by two possible binding routes (Fig. 6). In the first route, Frex binds two NADH molecules in a highly cooperative manner (Fig. 1). Thus, the intermediate with only one NADH molecule bound is hardly populated, and the fluorescent species $FrexN_2$ is instantaneously formed. Consequently, this step can be modelled as a single-step reaction characterized by a macroscopic dissociation constant $K_d \approx K_D^2$ (Fig. 1). The second route leads to the binding of one molecule NAD^+. Notably, this most simple reaction pattern builds on the assumption that other Frex adducts are virtually absent under equilibrium conditions. This premise is justified since (1) Frex can bind two nucleotides at the most, (2) the binding of two NAD^+ molecules is electrostatically hindered (McLaughlin et al. 2010), and (3) the formation of a mixed $FrexN^+N$ species is apparently disfavoured by the high affinity of Frex towards NADH and the pronounced cooperativity of the associated binding process. These assumptions and the derived

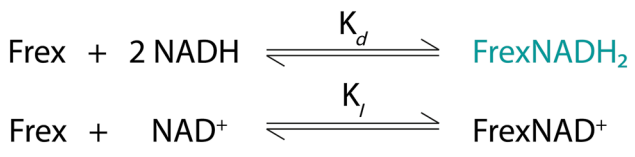

Fig. 6 Minimal model for Frex interaction with NADH or NAD^+. The fluorescence is assumed to be only generated by the Frex species with two NADH molecules bound ($FrexNADH_2$, *teal* colour)

minimal model (Fig. 6) lead to an equation describing the observed fluorescence in dependency of [N] and [N^+] (see "Appendix" for derivation):

$$F = \frac{F_{\max}[\mathrm{N}]^2}{K_d + [\mathrm{N}]^2 + \frac{[\mathrm{N}^+]K_d}{K_I}}. \tag{5}$$

Here, F is the fluorescence amplitude for given substrate and inhibitor concentrations, while $F_{\max}$ is the maximal fluorescence amplitude (at saturating [NADH], with no NAD^+ present). The apparent affinity for Frex towards two molecules of NADH and one molecule of NAD^+ is reflected by the reciprocal of the dissociation constants K_d and K_I, respectively. Rearrangement of Eq. 5 for $F_{\max}/F$ yields

$$\frac{F_{\max}}{F} = \frac{K_d}{[\mathrm{N}]^2} + 1 + \frac{[\mathrm{N}^+]K_d}{K_I[\mathrm{N}]^2}, \tag{6}$$

which is a linear function of [NAD^+] with a *y-axis* intercept of $y = 1 + \frac{K_d}{[\mathrm{N}]^2}$ and a slope of $\frac{K_d}{K_I[\mathrm{N}]^2}$. Data obtained by the titration of Frex with NAD^+ at two different fixed concentrations of NADH were plotted as $F_{\max}/F$ versus [NAD^+], yielding a linear dependence, which was fitted according to Eq. 6 (Fig. 7).

The apparent dissociation constant K_I of the inhibitor NAD^+ was approximated by fitting the data obtained in the presence of 15 µM NADH by Eq. 6. The *y-axis* intercept was used to substitute the term $K_d/[\mathrm{N}]^2$ in the slope, leading to $K_I \approx 400$ µM (at 20 °C).

Starting from Eq. 6, we also obtained an expression that relates the squared NADH concentration to the fluorescence readout:

$$[\mathrm{N}]^2 = \frac{K_dK_I + K_d[\mathrm{N}^+]}{K_I\left(\frac{F_{\max}-F}{F}\right)}. \tag{7}$$

If $[\mathrm{N}^+] \ll K_I$, this equation simplifies to

$$[\mathrm{N}] = \sqrt{\left(\frac{F}{F_{\max}-F}\right)K_d}, \tag{8}$$

which represents the minimum NADH concentration reflected by a given fluorescence readout. In principle,

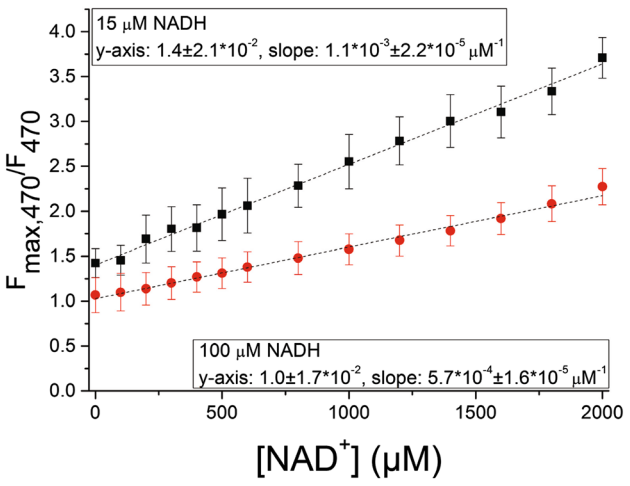

Fig. 7 NAD^+-dependent Frex fluorescence emission plotted as F_{max}/F obtained upon excitation at 470 nm in the presence of 15 µM NADH (*black*) and 100 µM NADH (*red*) at 20 °C. Results of a linear fit to the data are superimposed (*dashed black lines*) with fit parameters given in the *insets*

Eq. 7 could also report on [N] in the presence of NAD^+. However, the applicability of this expression is somewhat limited, since the decrease of the sensor's dynamic range in the presence of NAD^+ (F never reaches F_{max}, see Fig. 1b) is not explicitly included in our minimal model (Fig. 6). Specifically, this observation indicates that Frex inhibition by NAD^+ is not purely competitive in character, which can be rationalized by the fact that NAD^+ shares its binding site with only one of the two NADH molecules. Thus, it would be advantageous to extend the minimal mechanism by untangling the cooperative binding of the two NADH molecules. This, however, requires quantifying species with only one NADH molecule bound, a challenge that is left for future studies.

In a more recent publication, a new fluorescence sensor for NAD(H) was designed in such way, that it independently responds towards NAD^+ and NADH. This sensor, termed SoNar, may be a promising alternative to quantitatively monitor nucleotide levels in bacterial cells and mitochondria (Zhao et al. 2015).

pH dependence

Introducing Frex as a fluorescent probe, Zhao et al. mentioned the pH sensitivity of the sensor and the resulting need to calibrate its signal for possible pH changes of the investigated medium (Zhao et al. 2011). The pH dependence of fluorescence has already been described for cpYFP itself (Schwarzländer et al. 2014) and other derived sensors (Nagai et al. 2001). The response of Frex towards pH changes between pH 7 and pH 10.5 has been shown to be considerable, and at high pH, fluorescence increases dramatically and even reaches much higher absolute levels than in the presence of saturating [NADH] in the absence of NAD^+ at pH 7.4 (see Figs. 1, 5). This has to be considered for in vivo applications of this sensor; even though pH is tightly regulated within cells, it can vary due to external factors (Olsen et al. 2002). Unfortunately, already slight differences can falsify the fluorescence readout of the sensor. This can be explained by the fact that cpYFP is even more pH sensitive in the physiological pH regime than YFP itself (Llopis et al. 1998; Schwarzländer et al. 2014). Therefore, Zhao et al. proposed to consider pH deviations by normalizing the Frex fluorescence using the cpYFP readout obtained from a comparable sample (Zhao et al. 2011). Also other biosensors like eGFP-pHsens can be co-expressed for strict pH monitoring (Schmitt et al. 2014b). Nonetheless, this procedure is laborious, and a more straightforward approach to Frex utilization would be desirable.

Since the pH dependency of fluorescence intensities arises from two different chromophore species, it would be advisable to selectively stabilize one of them, preferably the alkaline form, to (1) ultimately exploit a higher dynamic range and (2) eliminate the pH dependency at physiological pH levels (Chattoraj et al. 1996). For cpYFP, a pK_a of 8.9 has been reported, and the value for Frex might be comparable (Griesbeck et al. 2001). In order to obtain only the deprotonated species at a physiological pH of 7.4, it is necessary to shift the sensor's pK_a to smaller values by at least 3.5 units. A similar procedure has already been established in the Citrine variant of YFP, in which the Gln69Met substitution led to a lowered pK_a and a decreased chloride sensitivity of the sensor (Day and Davidson 2009), suggesting that there might be potential for improvement of the Frex sensor. In the case of cpYFP, the Citrine variant also shows a lowered pK_a, which, however, is close to physiological pH (7.7). Thus, cpCitrine is very sensitive towards pH changes in the physiological range, and therefore, the protein would be even less suited for applications in vivo (Griesbeck et al. 2001). Consequently, in order to obtain a pH-insensitive high-dynamic-range sensor, further efforts are necessary to obtain mutant proteins exhibiting a more pronounced pK_a shift.

Conclusions

- In contrast to previous reports, the effect of NAD^+ on Frex fluorescence cannot be neglected under in vivo conditions.

- The effect of NAD^+ binding on NADH sensing by Frex seems to be a mixed inhibition mechanism, with both non-competitive and competitive characteristics.
- Frex allows estimating a minimum NADH concentration, if $[NAD^+]$ is small compared to the dissociation constant for NAD^+ binding.
- The pH and temperature sensitivity of the Frex fluorescence can strongly interfere with NAD(H) sensing in vivo.
- In total, the in vivo application of the sensor in its current state is complicated by its multifactorial fluorescence response.
- Further genetic engineering of the sensor's pK_a could elevate its dynamic range and decrease its pH dependency under physiological conditions.
- Untangling the cooperative binding of two NADH molecules could extend the mechanistic understanding and the sensor's applicability.

Acknowledgements The authors are grateful to Dr. William Oldham and Prof. Joseph Loscalzo (Harvard Medical School, USA) for providing the Frex(H) expression clones. This work was supported by the German Research Foundation—Cluster of Excellence "Unifying Concepts in Catalysis" (to S.W., M.H., T.F., I.Z., and O.L.).

Appendix

Model for NADH binding and the derivation of K_d

The binding of two NADH molecules to Frex can be described as

$$\mathrm{Frex} + 2\mathrm{NADH} \overset{K_{D,1}}{\longleftrightarrow} \mathrm{FrexN} + \mathrm{NADH} \overset{K_{D,2}}{\longleftrightarrow} \mathrm{FrexN_2}$$

For this process, the macroscopic dissociation constant is a product of two microscopic constants, and we shortly denote this product as $K_d = K_{D,1} \times K_{D,2}$. In the Hill fit, we determine the averaged single-step dissociation constant K_D (in the absence of NAD^+), and the highly cooperative character of NADH binding leads to the valid approximation $K_d \approx K_D^2$. FrexN and $\mathrm{FrexN_2}$ refer to Frex with one and two bound NADH molecules, respectively.

Derivation of an equation for inhibition

A model for the inhibition of Frex by NAD^+ is presented in Fig. 6. If we assume that the fluorescence (F) is only emitted by the species $\mathrm{FrexN_2}$, i.e. Frex bound to two NADH molecules, F relates to the fraction of $\mathrm{FrexN_2}$ by

$$F \sim \frac{[\mathrm{FrexN_2}]}{[\mathrm{Frex}] + [\mathrm{FrexN_2}] + [\mathrm{FrexN^+}]}. \tag{9}$$

Expanding by 1/[Frex] leads to

$$F \sim \frac{\frac{[\mathrm{FrexN_2}]}{[\mathrm{Frex}]}}{1 + \frac{[\mathrm{FrexN_2}]}{[\mathrm{Frex}]} + \frac{[\mathrm{FrexN^+}]}{[\mathrm{Frex}]}}. \tag{10}$$

For the two different reactions, the law of mass action yields

$$K_d = \frac{[\mathrm{Frex}][\mathrm{N}]^2}{[\mathrm{FrexN_2}]} \tag{11}$$

and

$$K_I = \frac{[\mathrm{Frex}][\mathrm{N^+}]}{[\mathrm{FrexN^+}]}. \tag{12}$$

If we substitute the quotients in Eq. 10 by these expressions, we obtain

$$F \sim \frac{\frac{[\mathrm{N}]^2}{K_d}}{1 + \frac{[\mathrm{N}]^2}{K_d} + \frac{[\mathrm{N^+}]}{K_I}}. \tag{13}$$

Expansion with K_d yields

$$F \sim \frac{[\mathrm{N}]^2}{K_d + [\mathrm{N}]^2 + \frac{[\mathrm{N^+}]K_d}{K_I}} \tag{14}$$

and inclusion of a constant to normalize for the maximum fluorescence ($F_{\max}$) results in Eq. 15, which equals Eq. 5 that was used to fit the fluorescence data shown in Fig. 7 by its linearized variant $F_{\max}/F$:

$$F = \frac{F_{\max}[\mathrm{N}]^2}{K_d + [\mathrm{N}]^2 + \frac{[\mathrm{N^+}]K_d}{K_I}}. \tag{15}$$

References

Baird GS, Zacharias DA, Tsien RY (1999) Circular permutation and receptor insertion within green fluorescent proteins. Proc Natl Acad Sci U S A 96:11241–11246. doi:10.1073/pnas.96.20.11241

Bennett B, Kimball E, Gao M (2009) Absolute metabolite concentrations and implied enzyme active site occupancy in *Escherichia coli*. Nat Chem Biol 5:593–599. doi:10.1038/nchembio.186.Absolute

Bilan DS, Belousov VV (2016) Genetically encoded probes for NAD+/NADH monitoring. Free Radic Biol Med. doi:10.1016/j.freeradbiomed.2016.06.018

Bilan DS, Matlashov ME, Schultz C et al (2014) Genetically encoded fluorescent indicator for imaging NAD+/NADH ratio changes in different cellular compartments. Biochim Biophys Acta 1840:951–957. doi:10.1016/j.bbagen.2013.11.018.Genetically

Blacker TS, Mann ZF, Gale JE et al (2014) Separating NADH and NADPH fluorescence in live cells and tissues using FLIM. Nat Commun 5:3936. doi:10.1038/ncomms4936

Brekasis D, Paget MSB (2003) A novel sensor of NADH/NAD+ redox poise in Streptomyces coelicolor A3(2). EMBO J 22:4856–4865

Chattoraj M, King BA, Bublitz GU, Boxer SG (1996) Ultra-fast excited state dynamics in green fluorescent protein: multiple states and proton transfer. Proc Natl Acad Sci USA 93:8362–8367. doi:10.1073/pnas.93.16.8362

Day RN, Davidson MW (2009) The fluorescent protein palette: tools for cellular imaging. Chem Soc Rev 38:2887–2921. doi:10.1039/b901966a

Griesbeck O, Baird GS, Campbell RE et al (2001) Reducing the environmental sensitivity of yellow fluorescent protein: mechanism and applications. J Biol Chem 276:29188–29194. doi:10.1074/jbc.M102815200

Gyan S, Shiohira Y, Sato I et al (2006) Regulatory loop between redox sensing of the NADH/NAD+ ratio by Rex (YdiH) and oxidation of NADH by NADH dehydrogenase Ndh in *Bacillus subtilis*. J Bacteriol 188:7062–7071. doi:10.1128/JB.00601-06

Hung YP, Albeck JG, Tantama M, Yellen G (2011) Imaging cytosolic NADH-NAD+ redox state with a genetically encoded fluorescent biosensor. Cell Metab 14:545–554. doi:10.1016/j.cmet.2011.08.012

Larsson JT, Rogstam A, von Wachenfeldt C (2005) Coordinated patterns of cytochrome bd and lactate dehydrogenase expression in *Bacillus subtilis*. Microbiology 151:3323–3335. doi:10.1099/mic.0.28124-0

Lenz O, Lauterbach L, Frielingsdorf S, Friedrich B (2015) Oxygen-tolerant hydrogenases and their biotechnological potential. Biohydrogen 61–96. doi:10.1515/9783110336733.61

Lin SJ, Guarente L (2003) Nicotinamide adenine dinucleotide, a metabolic regulator of transcription, longevity and disease. Curr Opin Cell Biol 15:241–246. doi:10.1016/S0955-0674(03)00006-1

Llopis J, McCaffery JM, Miyawaki A et al (1998) Measurement of cytosolic, mitochondrial, and golgi pH in single living cells with green fluorescent proteins. Proc Natl Acad Sci 95:6803–6808. doi:10.1073/pnas.95.12.6803

McLaughlin KJ, Strain-Damerell CM, Xie K et al (2010) Structural basis for NADH/NAD+ redox sensing by a Rex family repressor. Mol Cell 38:563–575. doi:10.1016/j.molcel.2010.05.006

Nagai T, Sawano A, Park ES, Miyawaki A (2001) Circularly permuted green fluorescent proteins engineered to sense Ca^{2+}. Proc Natl Acad Sci USA 98:3197–3202. doi:10.1073/pnas.051636098

Olsen KN, Budde BB, Siegumfeldt H, Bjo K (2002) Noninvasive measurement of bacterial intracellular pH on a single-cell level with green fluorescent protein and fluorescence ratio imaging microscopy noninvasive measurement of bacterial intracellular pH on a single-cell level with green fluorescent prote. Appl Environ Microbiol 68:11–14. doi:10.1128/AEM.68.8.4145

Patterson GH, Knobel SM, Arkhammar P et al (2000) Separation of the glucose-stimulated cytoplasmic and mitochondrial NAD(P)H responses in pancreatic islet beta cells. Proc Natl Acad Sci USA 97:5203–5207. doi:10.1073/pnas.090098797

Rocheleau JV, Head WS, Piston DW (2004) Quantitative NAD(P)H/flavoprotein autofluorescence imaging reveals metabolic mechanisms of pancreatic islet pyruvate response. J Biol Chem 279:31780–31787. doi:10.1074/jbc.M314005200

Schmitt FJ, Renger G, Friedrich T et al (2014a) Reactive oxygen species: Re-evaluation of generation, monitoring and role in stress-signaling in phototrophic organisms. Biochim Biophys Acta 1837:835–848. doi:10.1016/j.bbabio.2014.02.005

Schmitt FJ, Thaa B, Junghans C et al (2014b) EGFP-pHsens as a highly sensitive fluorophore for cellular pH determination by fluorescence lifetime imaging microscopy (FLIM). Biochim Biophys Acta 1837:1581–1593. doi:10.1016/j.bbabio.2014.04.003

Schwarzländer M, Wagner S, Ermakova YG et al (2014) The "mito-flash" probe cpYFP does not respond to superoxide. Nature 514:E12–E14. doi:10.1038/nature13858

Sickmier EA, Brekasis D, Paranawithana S et al (2005) X-ray structure of a Rex-family repressor/NADH complex insights into the mechanism of redox sensing. Structure 13:43–54. doi:10.1016/j.str.2004.10.012

Tejwani V, Schmitt F-J, Wilkening S et al (2016) Investigation of the NADH/NAD+ ratio in Ralstonia eutropha using the fluorescence reporter protein peredox. Biochim Biophys Acta doi:10.1016/j.bbabio.2016.11.001

Wang E, Bauer MC, Rogstam A et al (2008) Structure and functional properties of the *Bacillus subtilis* transcriptional repressor Rex. Mol Microbiol 69:466–478. doi:10.1111/j.1365-2958.2008.06295.x

Yacoby I, Pochekailov S, Toporik H et al (2011) Photosynthetic electron partitioning between [FeFe]-hydrogenase and ferredoxin: NADP þ-oxidoreductase (FNR) enzymes in vitro. Pnas 108:9396–9401. doi:10.1073/pnas.1103659108/-/DCSupplemental.www.pnas.cgi/doi/10.1073/pnas.1103659108

Ying W (2008) NAD+/NADH and NADP+/NADPH in cellular functions and cell death: regulation and biological consequences. Antioxid Redox Signal 10:179–206. doi:10.1089/ars.2007.1672

Zhao Y, Jin J, Hu Q et al (2011) Genetically encoded fluorescent sensors for intracellular NADH detection. Cell Metab 14:555–566. doi:10.1016/j.cmet.2011.09.004

Zhao Y, Hu Q, Cheng F et al (2015) SoNar, a highly responsive NAD+/NADH sensor, allows high-throughput metabolic screening of anti-tumor agents. Cell Metab 21:777–789. doi:10.1016/j.cmet.2015.04.009

Zhao Y, Wang A, Zou Y et al (2016) In vivo monitoring of cellular energy metabolism using SoNar, a highly responsive sensor for NAD+/NADH redox state. Nat Protoc 11:1345–1359. doi:10.1038/nprot.2016.074

Zhou Y, Wang L, Yang F et al (2011) Determining the extremes of the cellular NAD(H) level by using an *Escherichia coli* NAD+-auxotrophic mutant. Appl Environ Microbiol 77:6133–6140. doi:10.1128/AEM.00630-11